Supporting Information

Selective and cell-active PBRM1 bromodomain inhibitors discovered through NMR fragment screening

Shifali Shishodia,[1],* Raymundo Nuñez,[1] Brayden P. Strohmier,[2] Karina L. Bursch,[1] Christopher J. Goetz,[1] Michael D. Olp,[1] Davin R. Jensen,[1] Tyler G. Fenske,[1] Sandra C. Ordonez-Rubiano,[2] Maya E. Blau,[1] Mallory K. Roach,[2] Francis C. Peterson,[1] Brian F. Volkman,[1] Emily C. Dykhuizen,[2] Brian C. Smith[1],*

[1]Department of Biochemistry, Program in Chemical Biology, Medical College of Wisconsin, Milwaukee, WI 53226, United States
[2]Department of Medicinal Chemistry and Molecular Pharmacology, Purdue University, West Lafayette, IN 47907, United States
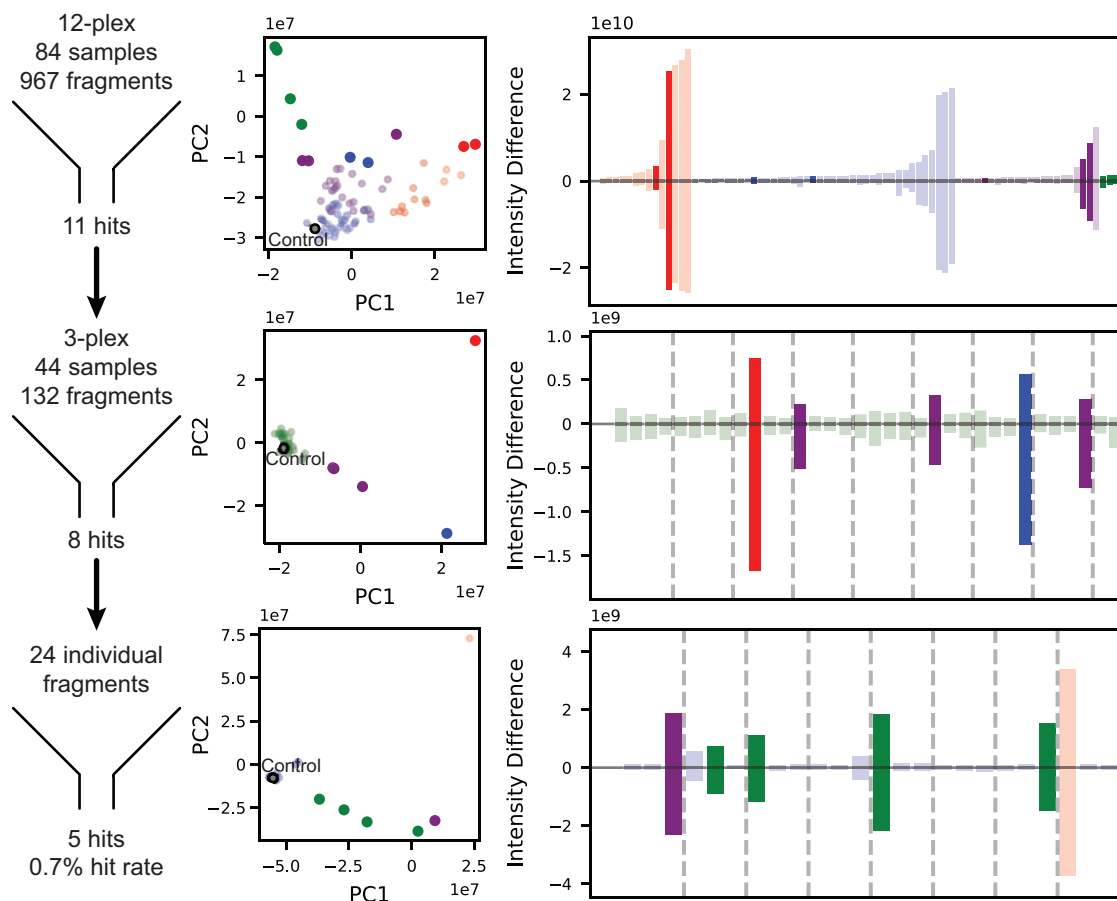
*Shifali Shishodia. Email: sshishodia@mcw.edu
*Brian C. Smith. Email: brismith@mcw.edu

Supplementary Figures and Tables

Figure S1. Summary of protein-detected NMR-based fragment screen of the Zenobia Library targeting PBRM1-BD2. 967 fragments were screened in pools of 12, 3, or individual compounds, and hits were identified through stepwise parsing of selected samples, yielding a final hit rate of 0.7% (left column). At each stage of parsing, identification of hit samples was aided by principal component analysis (middle column) and difference intensity analysis (right column) of the 2D HMQC spectra. Samples are colored according to *k*-means clustering of principal components. Throughout the screening process, samples selected as hits are represented as solid circles and bars. Control samples in the PCA plots are represented as grey circles outlined black.
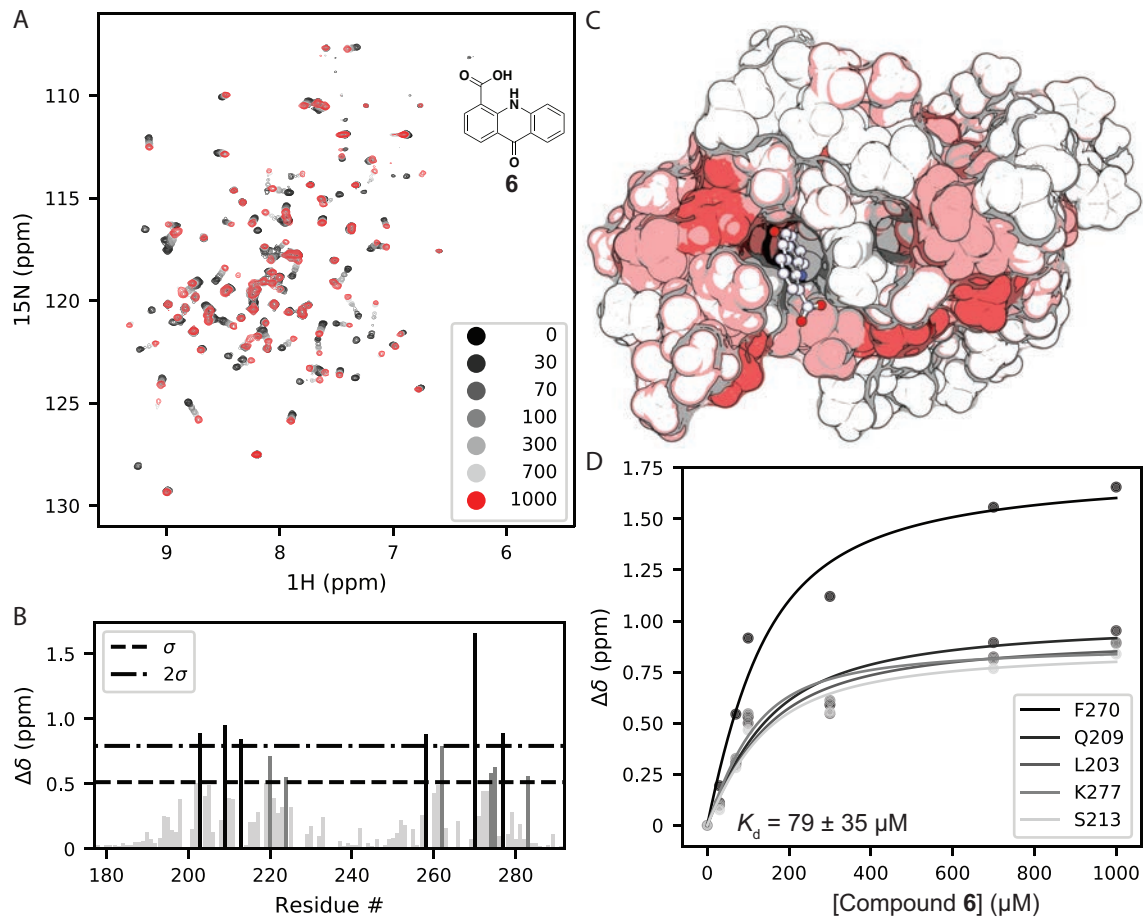
Figure S2. (A) ^{1}H, ^{15}N SOFAST-HMQC overlays of PBRM1-BD2 titrated with increasing concentrations of **6** (structure in insert). (B) Quantification of total chemical shift perturbations (^{1}H/^{15}N Δδ chemical shift) manifested by **6** (1 mM) for individual amino acid residues of PBRM1-BD2. (C) Mapping of substantially perturbed residues on the crystal structure of PBRM1-BD2 (PDB ID: 3LJW). The *in silico* docked pose of **6** into the active site of PBRM1-BD2 is included. Residues displaying CSPs >2σ (red), between 1σ and 2σ (pink), or <1σ (white) are indicated. (D) Concentration-response curves of indicated residues used to calculate binding affinity (K_d = 79 ± 35 μM) of **6** for PBRM1-BD2 using GraphPad Prism.
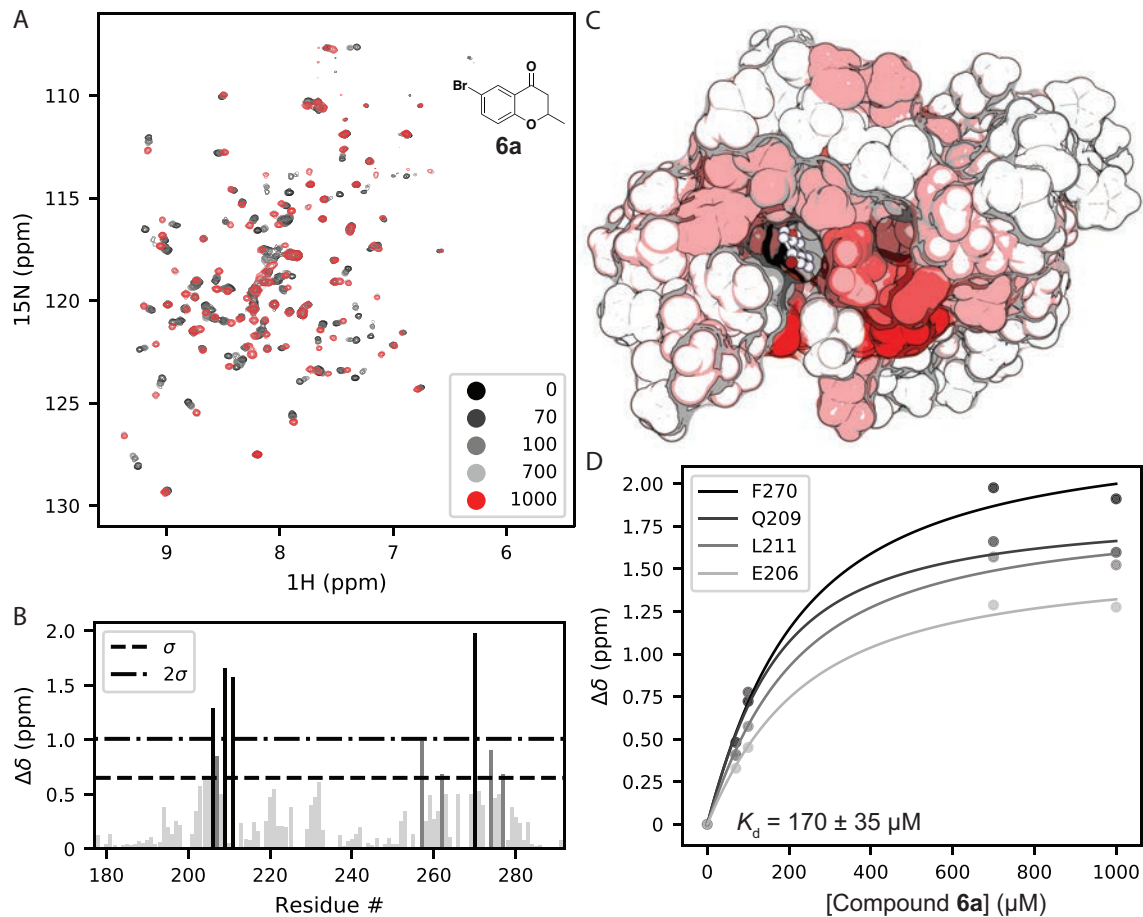
Figure S3. (A) ^{1}H, ^{15}N SOFAST-HMQC overlays of PBRM1-BD2 titrated with increasing concentrations of **6a** (structure in insert). (B) Quantification of total chemical shift perturbations (^{1}H/^{15}N Δδ chemical shift) manifested by **6a** (1 mM) for individual amino acid residues of PBRM1-BD2. (C) Mapping of substantially perturbed residues on the crystal structure of PBRM1-BD2 (PDB ID: 3LJW). The *in silico* docked pose of **6a** into the active site of PBRM1-BD2 is included. Residues displaying CSPs >2σ (red), between 1σ and 2σ (pink), or <1σ (white) are indicated. (D) Concentration-response curves of indicated residues used to calculate binding affinity ($K_d = 170 \pm 35$ μM) of **6a** for PBRM1-BD2 using GraphPad Prism.
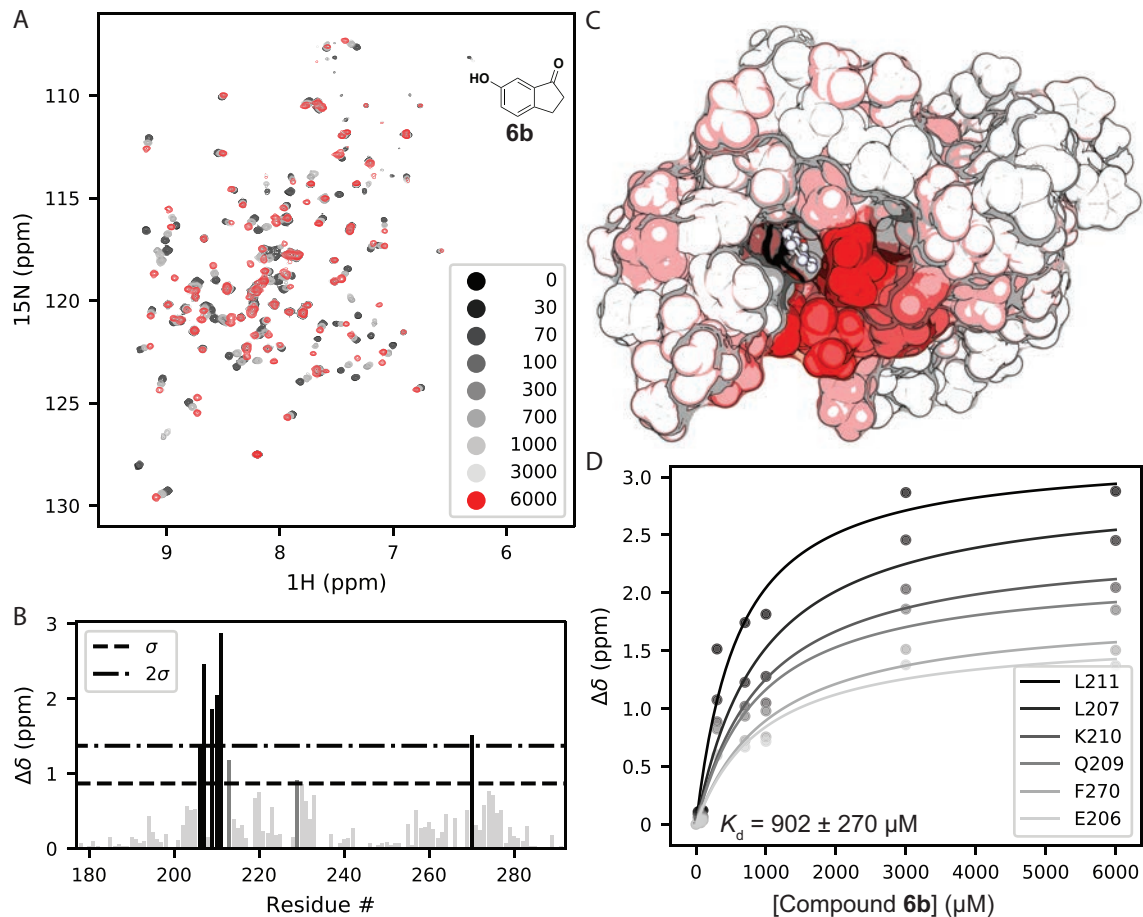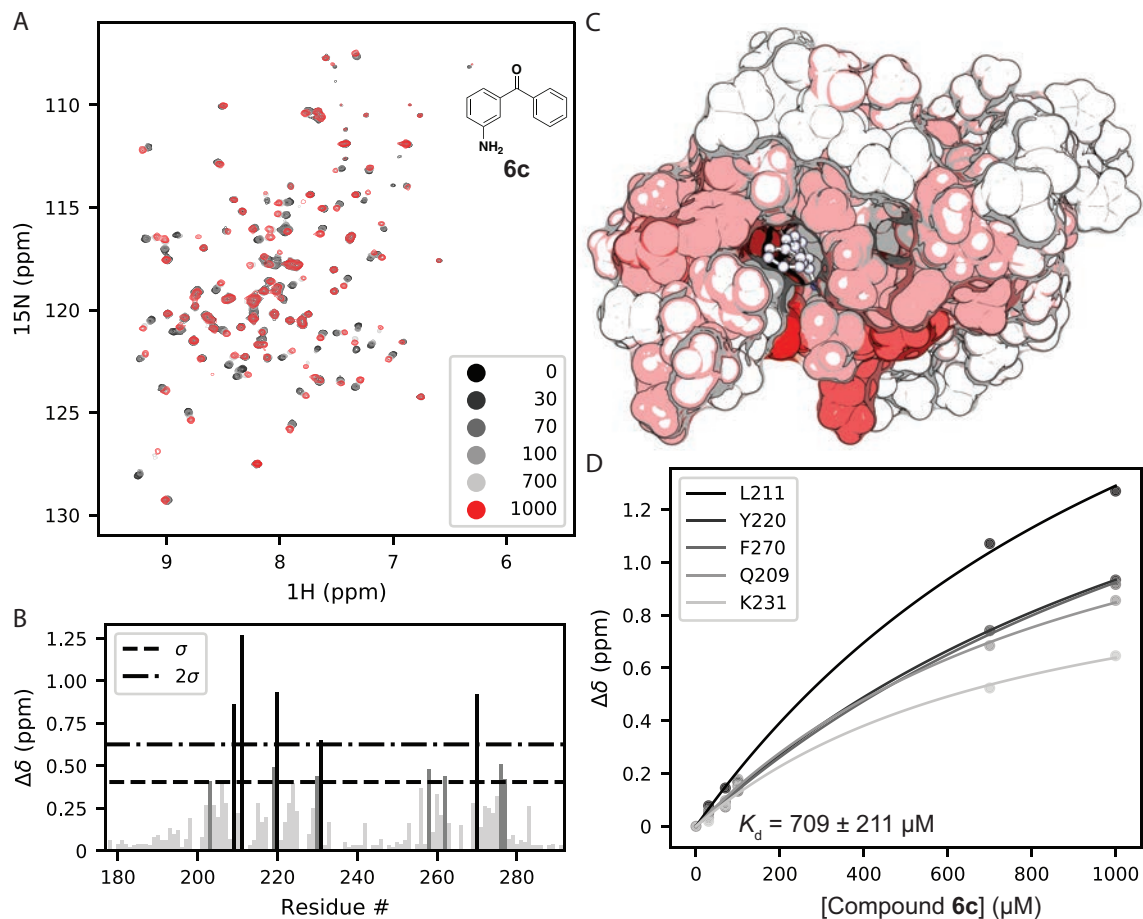
Figure S4. (A) ^{1}H, ^{15}N SOFAST-HMQC overlays of PBRM1-BD2 titrated with increasing concentrations of **6b** (structure in insert). (B) Quantification of total chemical shift perturbations (^{1}H/^{15}N $\Delta\delta$ chemical shift) manifested by **6b** (6 mM) for individual amino acid residues of PBRM1-BD2. (C) Mapping of substantially perturbed residues on the crystal structure of PBRM1-BD2 (PDB ID: 3LJW). The *in silico* docked pose of **6b** into the active site of PBRM1-BD2 is included. Residues displaying CSPs >2σ (red), between 1σ and 2σ (pink), or <1σ (white) are indicated. (D) Concentration-response curves of indicated residues used to calculate binding affinity (K_d = 902 ± 270 μM) of **6b** for PBRM1-BD2 using GraphPad Prism.
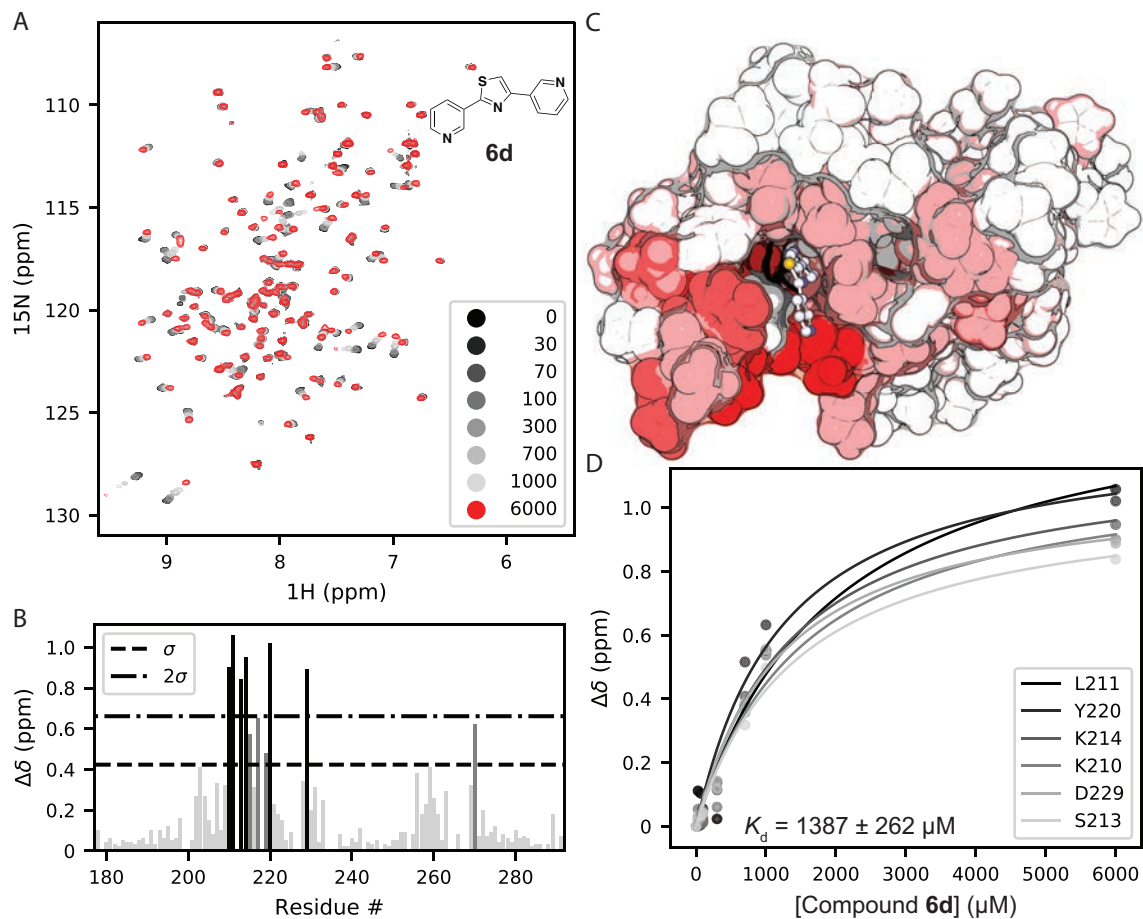
Figure S5. (A) ^{1}H, ^{15}N SOFAST-HMQC overlays of PBRM1-BD2 titrated with increasing concentrations of **6c** (structure in insert). (B) Quantification of total chemical shift perturbations (^{1}H/^{15}N Δδ chemical shift) manifested by **6c** (1 mM) for individual amino acid residues of PBRM1-BD2. (C) Mapping of substantially perturbed residues on the crystal structure of PBRM1-BD2 (PDB ID: 3LJW). The *in silico* docked pose of **6c** into the active site of PBRM1-BD2 is included. Residues displaying CSPs >2σ (red), between 1σ and 2σ (pink), or <1σ (white) are indicated. (D) Concentration-response curves of indicated residues used to calculate binding affinity ($K_d = 709 \pm 211$ μM) of **6c** for PBRM1-BD2 using GraphPad Prism.

Figure S6. (A) ^{1}H, ^{15}N SOFAST-HMQC overlays of PBRM1-BD2 titrated with increasing concentrations of **6d** (structure in insert). (B) Quantification of total chemical shift perturbations (^{1}H/[15]N Δδ chemical shift) manifested by **6d** (6 mM) for individual amino acid residues of PBRM1-BD2. (C) Mapping of substantially perturbed residues on the crystal structure of PBRM1-BD2 (PDB ID: 3LJW). The *in silico* docked pose of **6d** into the active site of PBRM1-BD2 is included. Residues displaying CSPs >2σ (red), between 1σ and 2σ (pink), or <1σ (white) are indicated. (D) Concentration-response curves of indicated residues used to calculate binding affinity (K_d = 1387 ± 262 μM) of **6d** for PBRM1-BD2 using GraphPad Prism.
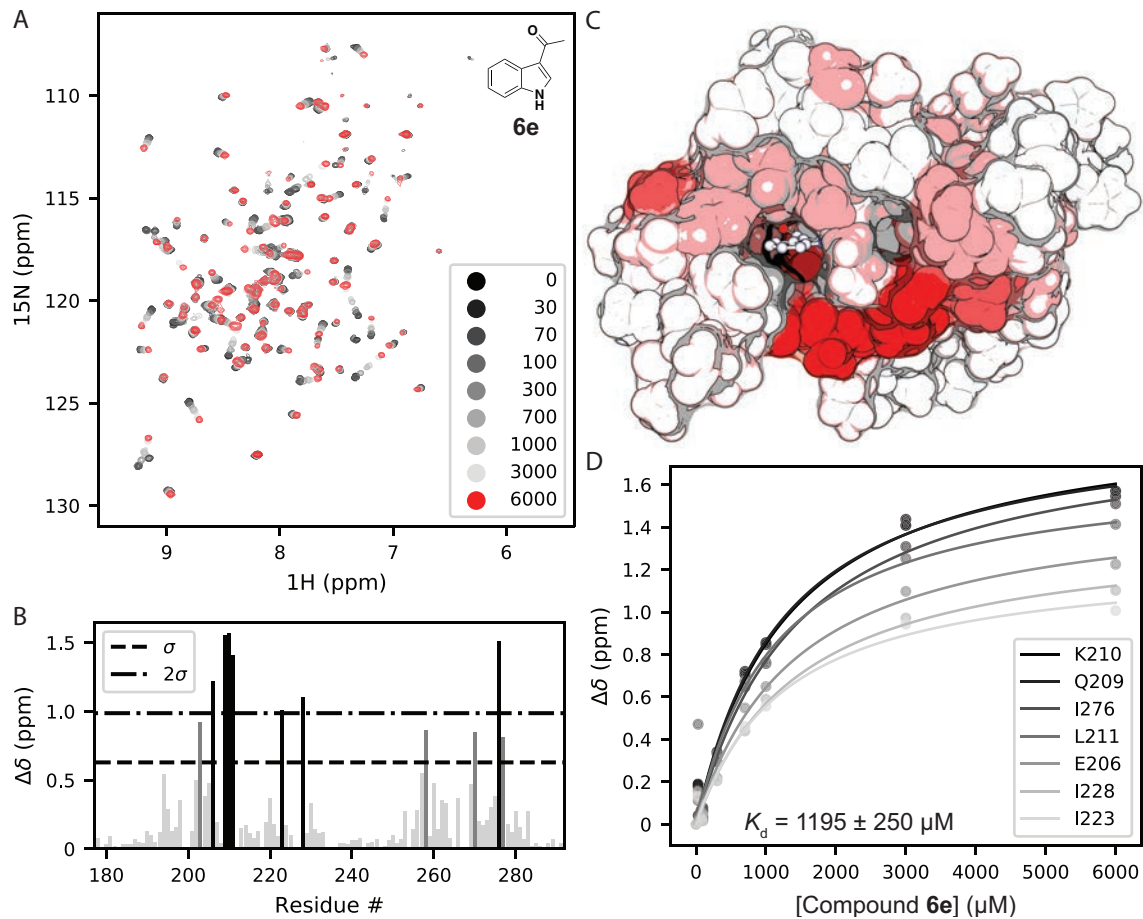
Figure S7. (A) ^{1}H, ^{15}N SOFAST-HMQC overlays of PBRM1-BD2 titrated with increasing concentrations of **6e** (structure in insert). (B) Quantification of total chemical shift perturbations (^{1}H/^{15}N $\Delta\delta$ chemical shift) manifested by **6e** (6 mM) for individual amino acid residues of PBRM1-BD2. (C) Mapping of substantially perturbed residues on the crystal structure of PBRM1-BD2 (PDB ID: 3LJW). The *in silico* docked pose of **6e** into the active site of PBRM1-BD2 is included. Residues displaying CSPs >2σ (red), between 1σ and 2σ (pink), or <1σ (white) are indicated. (D) Concentration-response curves of indicated residues used to calculate binding affinity ($K_d = 1195 \pm 250$ μM) of **6e** for PBRM1-BD2 using GraphPad Prism.

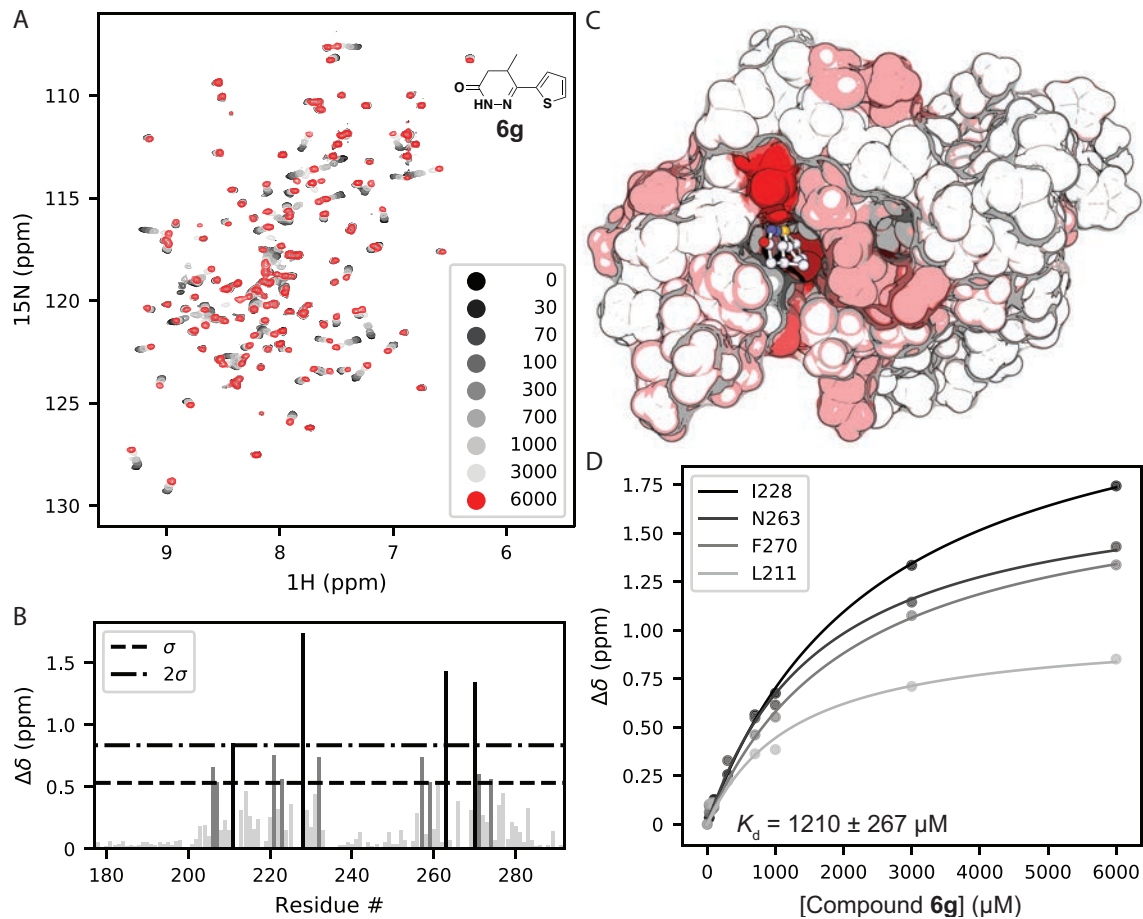**Figure S8.** (A) ^{1}H, ^{15}N SOFAST-HMQC overlays of PBRM1-BD2 titrated with increasing concentrations of **6g** (structure in inert). (B) Quantification of total chemical shift perturbations (^{1}H/[15]N $\Delta\delta$ chemical shift) manifested by **6g** (6 mM) for individual amino acid residues of PBRM1-BD2. (C) Mapping of substantially perturbed residues on the crystal structure of PBRM1-BD2 (PDB ID: 3LJW). The *in silico* docked pose of **6g** into the active site of PBRM1-BD2 is included. Residues displaying CSPs >2σ (red), between 1σ and 2σ (pink), or <1σ (white) are indicated. (D) Concentration-response curves of indicated residues used to calculate binding affinity (K_d = 1210 ± 267 µM) of **6g** for PBRM1-BD2 using GraphPad Prism.
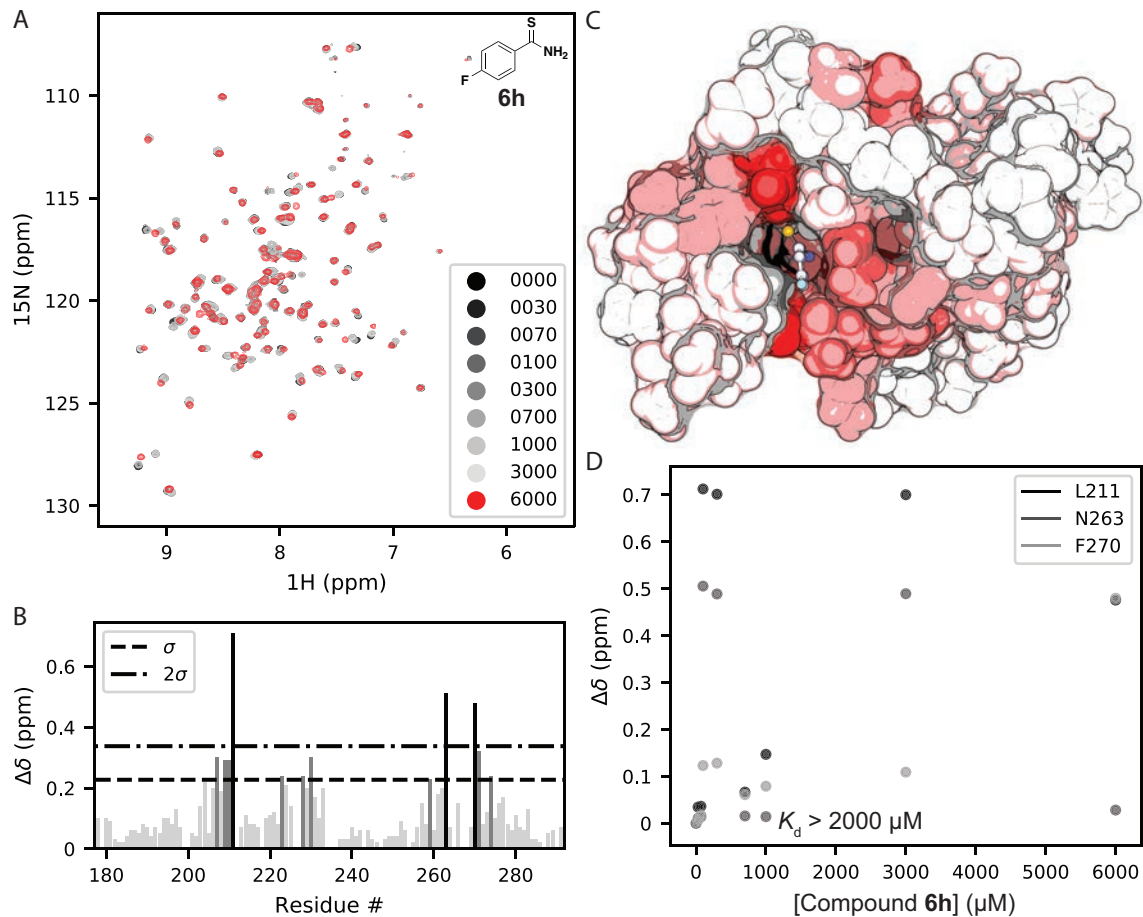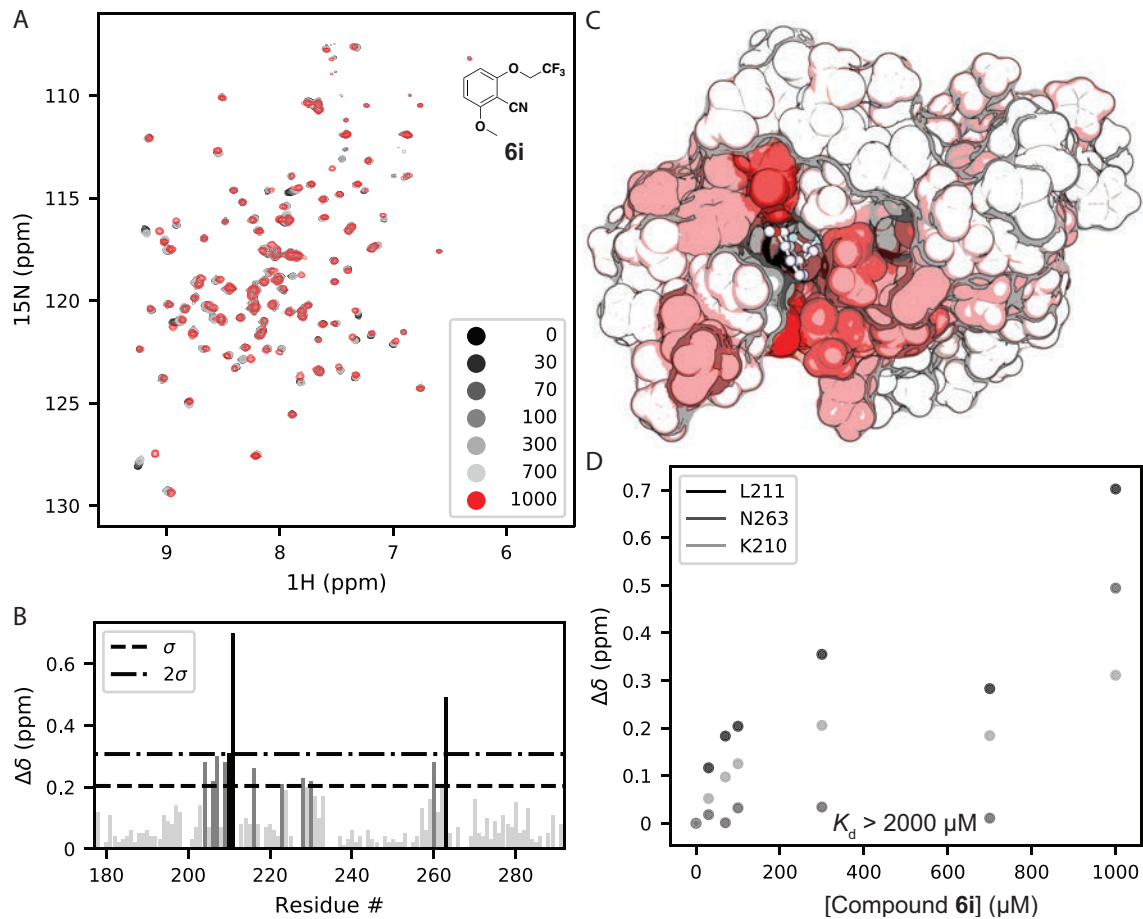
Figure S9. (A) ^{1}H, ^{15}N SOFAST-HMQC overlays of PBRM1-BD2 titrated with increasing concentrations of **6h** (structure in insert). (B) Quantification of total chemical shift perturbations (^{1}H/^{15}N $\Delta\delta$ chemical shift) manifested by **6h** (1 mM) for individual amino acid residues of PBRM1-BD2. (C) Mapping of substantially perturbed residues on the crystal structure of PBRM1-BD2 (PDB ID: 3LJW). The *in silico* docked pose of **6h** into the active site of PBRM1-BD2 is included. Residues displaying CSPs >2σ (red), between 1s and 2s (pink), or <1σ (white) are indicated. (D) Concentration-response curves of indicated residues used to calculate binding affinity (K_d > 2000 μM) of **6h** for PBRM1-BD2 using GraphPad Prism.

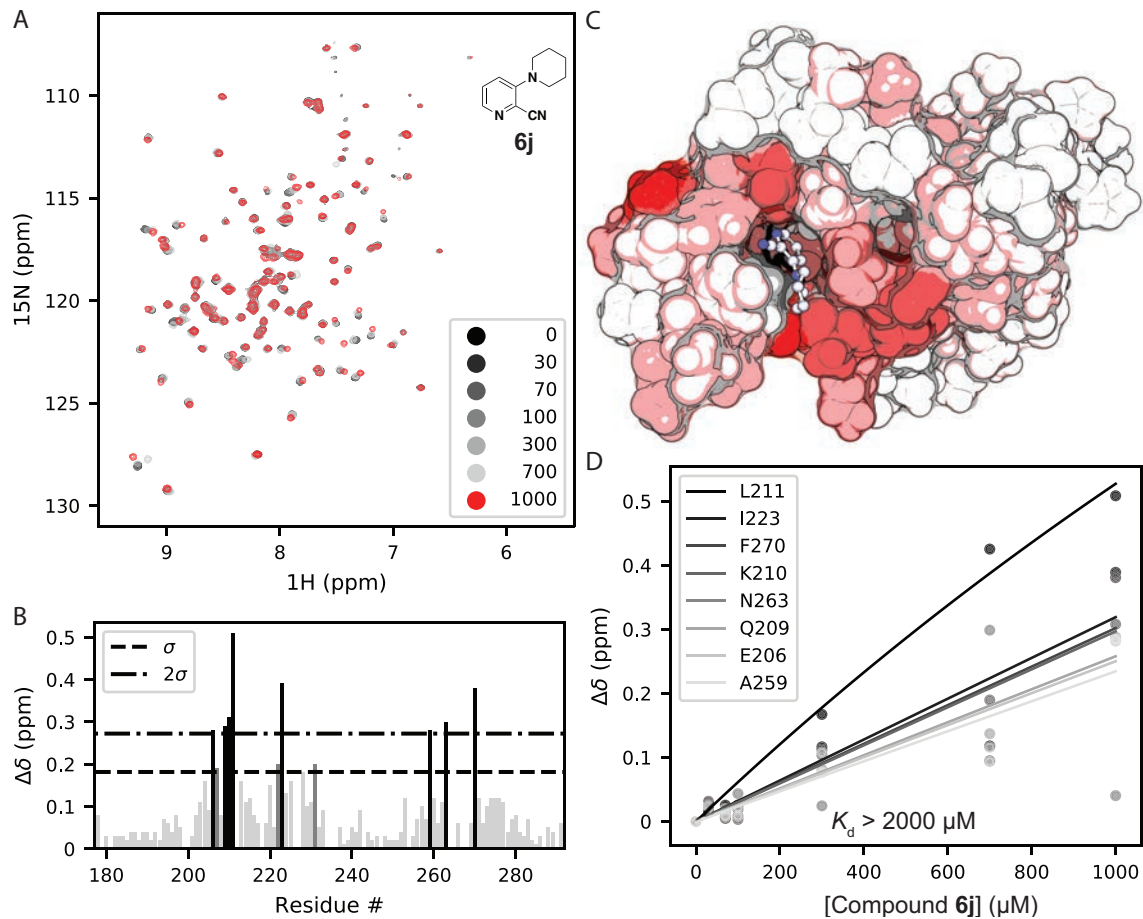**Figure S10.** (A) ^{1}H, ^{15}N SOFAST-HMQC overlays of PBRM1-BD2 titrated with increasing concentrations of **6i** (structure in insert). (B) Quantification of total chemical shift perturbations (^{1}H/[15]N Δδ chemical shift) manifested by **6i** (1 mM) for individual amino acid residues of PBRM1-BD2. (C) Mapping of substantially perturbed residues on the crystal structure of PBRM1-BD2 (PDB ID: 3LJW). The *in silico* docked pose of **6i** into the active site of PBRM1-BD2 is included. Residues displaying CSPs >2σ (red), between 1s and 2s (pink), or <1σ (white) are indicated. (D) Concentration-response curves of indicated residues used to calculate binding affinity ($K_d > 2000$ μM) of **6i** for PBRM1-BD2 using GraphPad Prism.
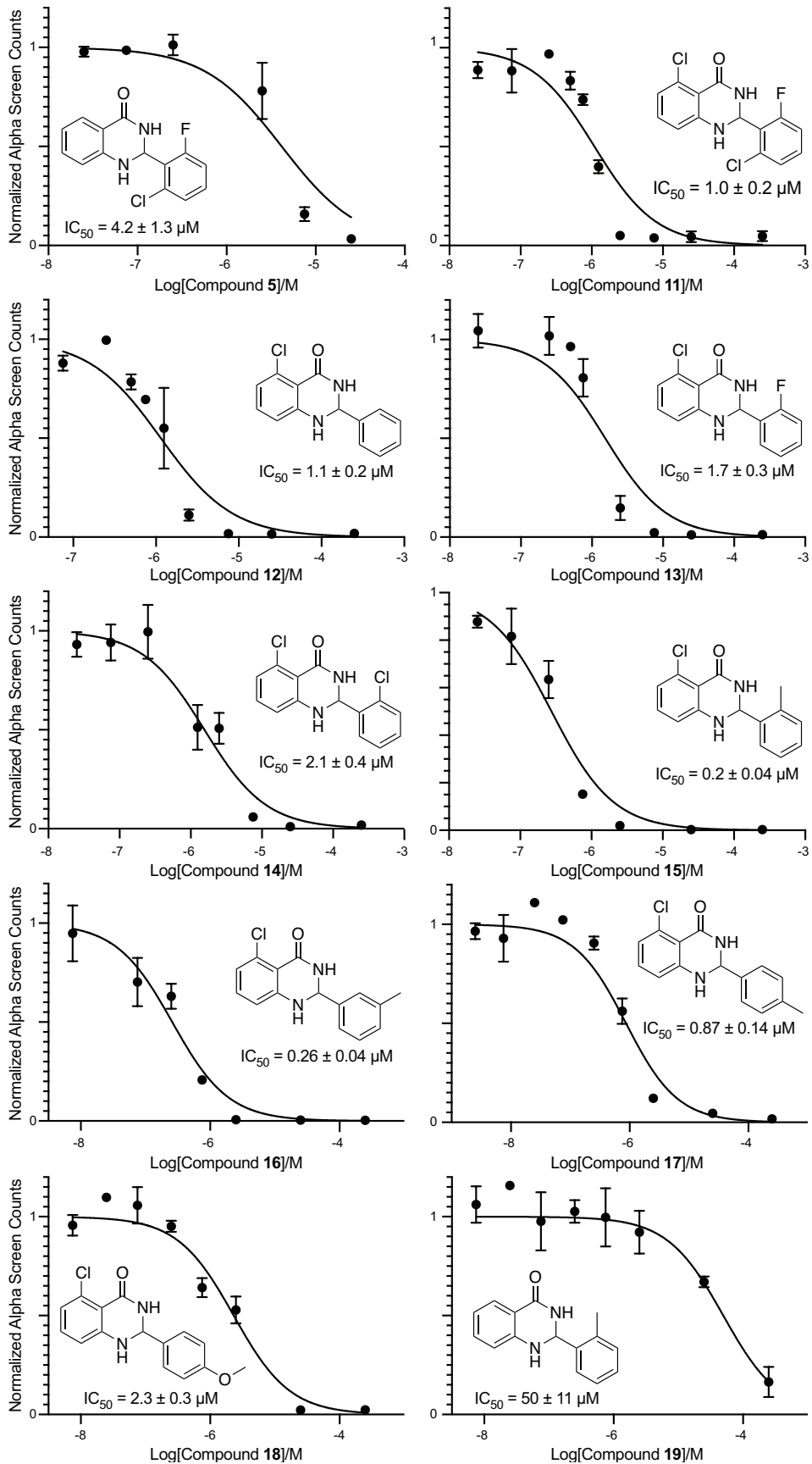
Figure S11. (A) ^{1}H, ^{15}N SOFAST-HMQC overlays of PBRM1-BD2 titrated with increasing concentrations of **6j** (structure in insert). (B) Quantification of total chemical shift perturbations (^{1}H/[15]N $\Delta\delta$ chemical shift) manifested by **6j** (1 mM) for individual amino acid residues of PBRM1-BD2. (C) Mapping of substantially perturbed residues on the crystal structure of PBRM1-BD2 (PDB ID: 3LJW). The *in silico* docked pose of **6j** into the active site of PBRM1-BD2 is included. Residues displaying CSPs >2σ (red), between 1σ and 2σ (pink), or <1σ (white) are indicated. (D) Concentration-response curves of indicated residues used to calculate binding affinity (K_d > 2000 μM) of **6j** for PBRM1-BD2 using GraphPad Prism.
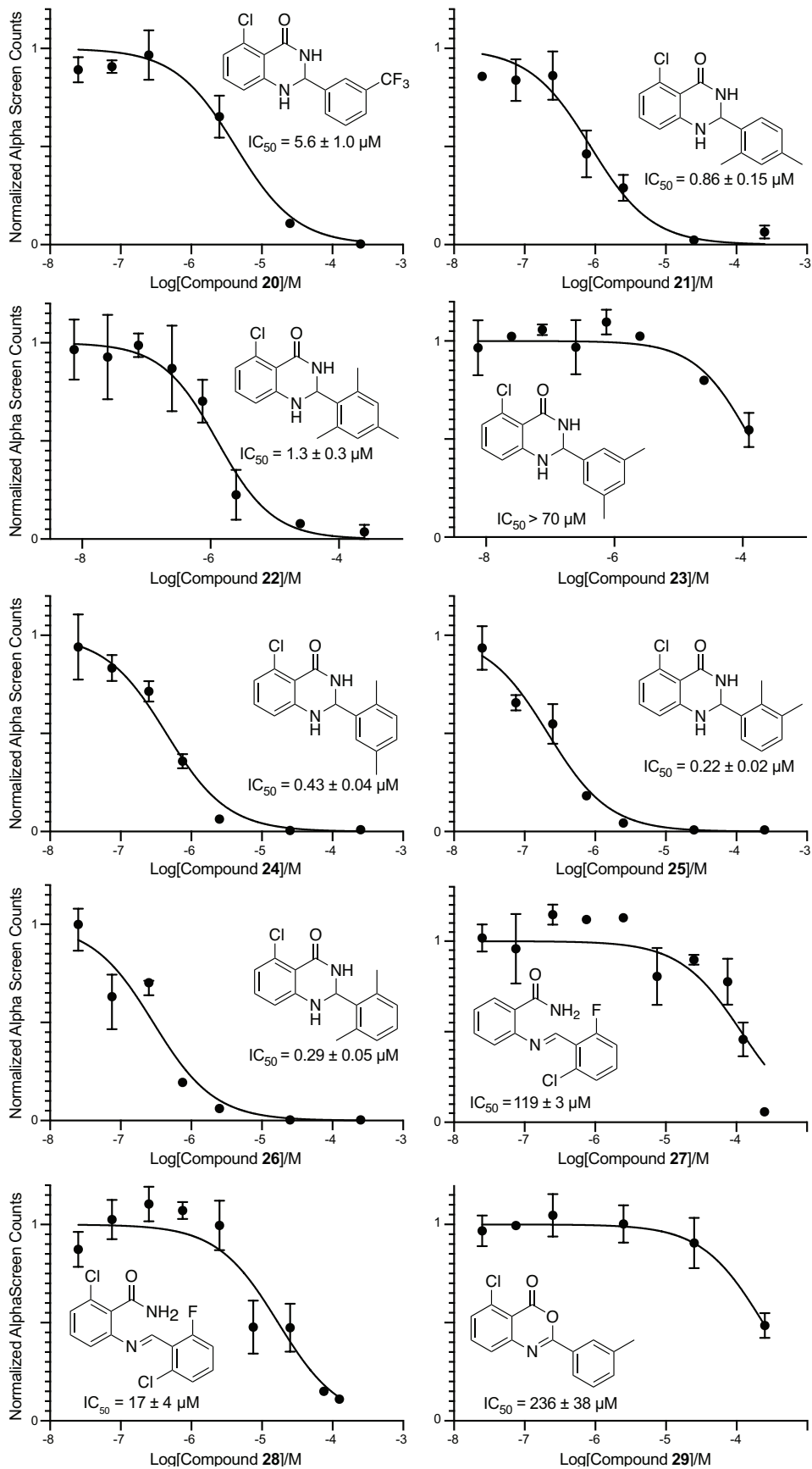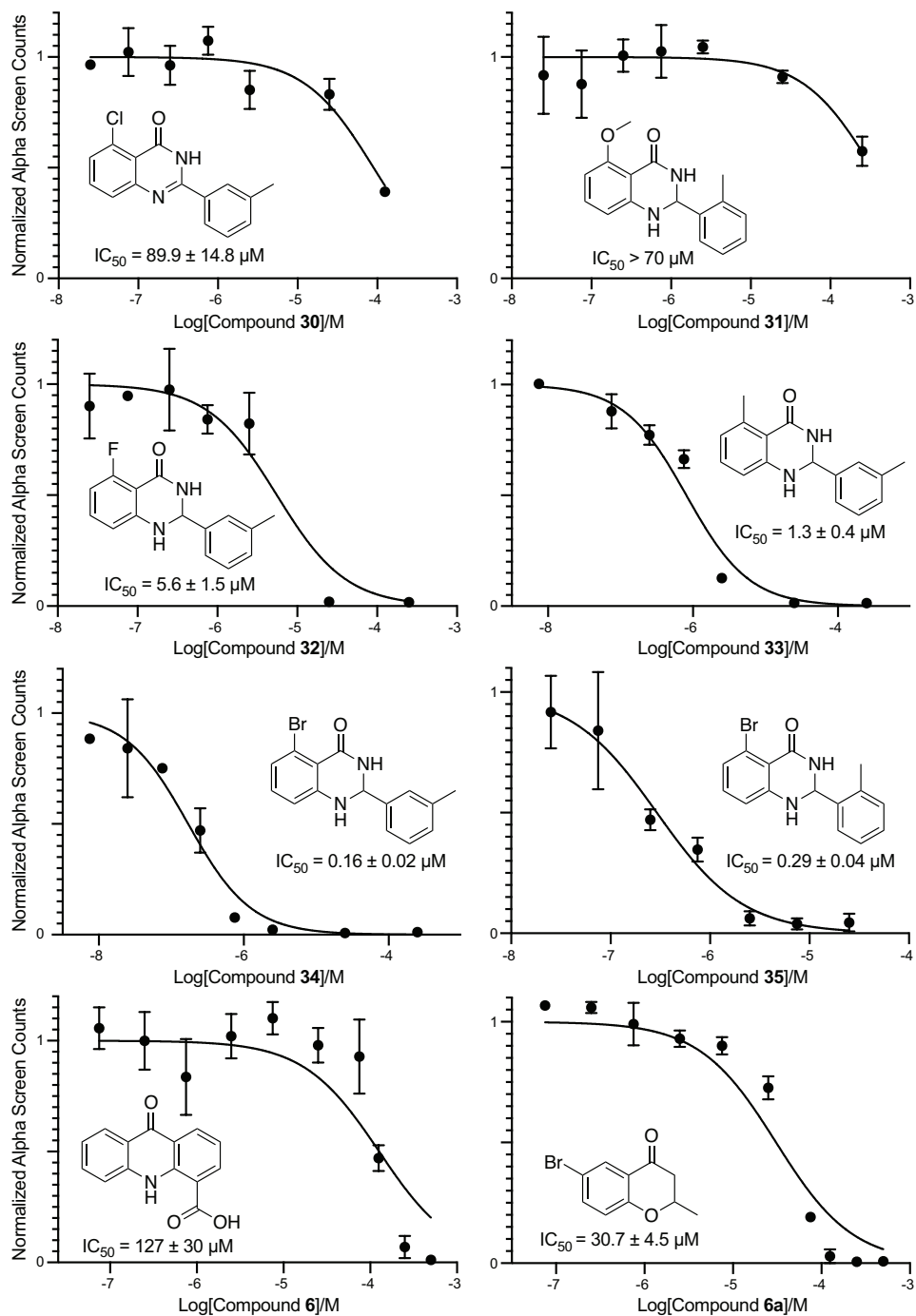
IC$_{50}$ = 4.2 ± 1.3 µM

IC$_{50}$ = 1.0 ± 0.2 µM

IC$_{50}$ = 1.1 ± 0.2 µM

IC$_{50}$ = 1.7 ± 0.3 µM

IC$_{50}$ = 2.1 ± 0.4 µM

IC$_{50}$ = 0.2 ± 0.04 µM

IC$_{50}$ = 0.26 ± 0.04 µM

IC$_{50}$ = 0.87 ± 0.14 µM

IC$_{50}$ = 2.3 ± 0.3 µM

IC$_{50}$ = 50 ± 11 µM

IC$_{50}$ = 5.6 ± 1.0 μM

Log[Compound **20**]/M

IC$_{50}$ = 0.86 ± 0.15 μM

Log[Compound **21**]/M

IC$_{50}$ = 1.3 ± 0.3 μM

Log[Compound **22**]/M

IC$_{50}$ > 70 μM

Log[Compound **23**]/M

IC$_{50}$ = 0.43 ± 0.04 μM

Log[Compound **24**]/M

IC$_{50}$ = 0.22 ± 0.02 μM

Log[Compound **25**]/M

IC$_{50}$ = 0.29 ± 0.05 μM

Log[Compound **26**]/M

IC$_{50}$ = 119 ± 3 μM

Log[Compound **27**]/M

IC$_{50}$ = 17 ± 4 μM

Log[Compound **28**]/M

IC$_{50}$ = 236 ± 38 μM

Log[Compound **29**]/M

Normalized Alpha Screen Counts

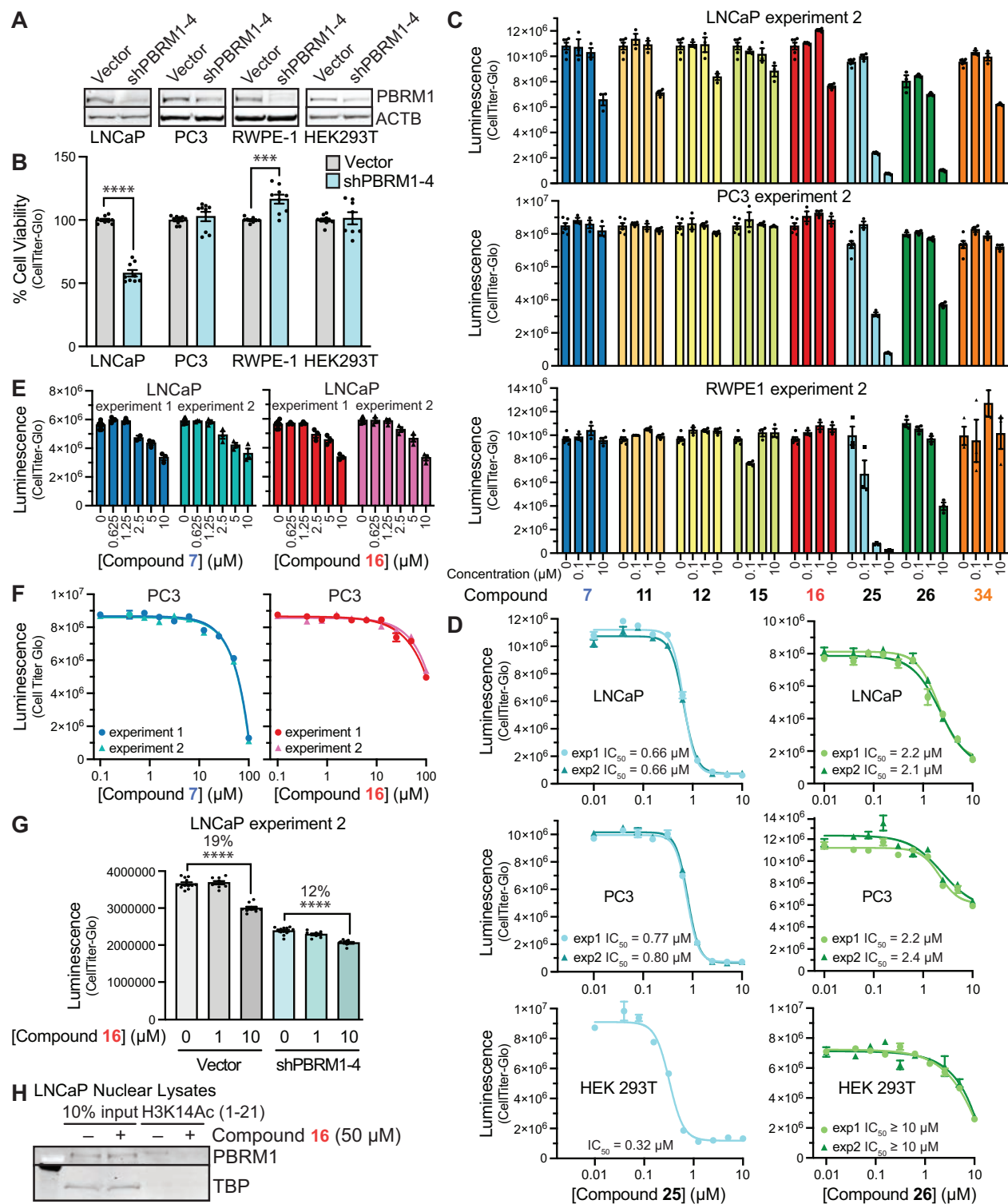Normalized AlphaScreen Counts

S15

Figure S12. IC$_{50}$ curves from AlphaScreen assays using 0.2 µM His$_6$-tagged PBRM1-BD2 and 0.1 µM biotinylated H3K14Ac (residues 1-20) peptide.

Figure S13. Cellular activity of PBRM1-BD2 inhibitors. (A) Immunoblot of lysates from human cell lines with lentiviral expression of shRNA against PBRM1 or vector control shRNA. (B) Cell viability after 6 days incubation of cell lines expressing lentiviral shPBRM1 or vector control. (C) Repeat of experiment in Figure 7C. Prostate cell line viability after 5 days treatment with 0, 0.1, 1, or 10 μM of indicated PBRM1 bromodomain inhibitors. Viability was measured as luminescence units using CellTiter-Glo®. n = 3 for

compound treatments; n = 6 for DMSO alone. (D) Concentrative curve measurement for compounds **25** and **26** treatment in LNCaP, PC3, and HEK293T cells. Assay performed as described in Figure S13A. IC$_{50}$ values were calculated from variable slope dose curve generated using GraphPad Prism. (E/F) Viability of (E) LNCaP and (F) PC3 prostate cancer cell lines treated with indicated concentrations of compounds **7** and **16**. Assay performed as described in S13A. (G) Repeat of experiment in Figure 7E. The viability of LNCaP cells expressing shRNA against *PBRM1* (shPBRM1) or vector control after 5 days treatment with 0, 1, or 10 µM compound **16.** Viability was measured as luminescence units using CellTiter-Glo®. n = 9-12; **** $p < 0.0001$. Significance calculated using Student's *t*-test. (H) Immunoblot analysis after streptavidin-mediated peptide pull-downs with biotinylated H3 or H3K14Ac peptide from LNCaP nuclear lysate containing 150 mM NaCl. Enrichment of PBRM1 and TATA binding protein (TBP) was determined by immunoblot analysis.
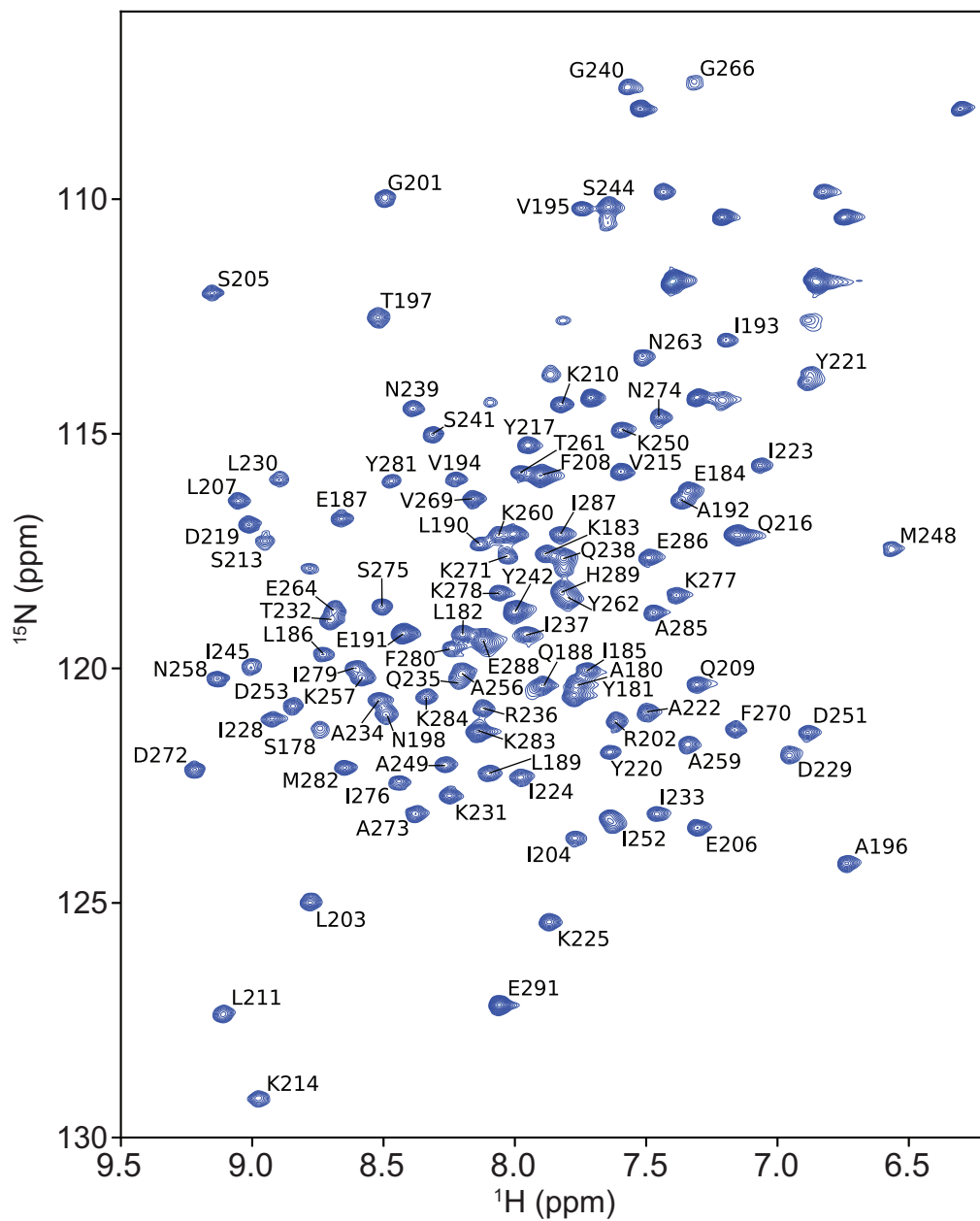
Figure S14. ^{1}H-^{15}N HSQC spectrum of apo U-^{15}N-PBRM1-BD2 (600 μM) with resonances labeled with their amino acid assignments. The chemical shifts for these assignments were deposited in the Biological Magnetic Resonance Bank (BMRB ID 51472).
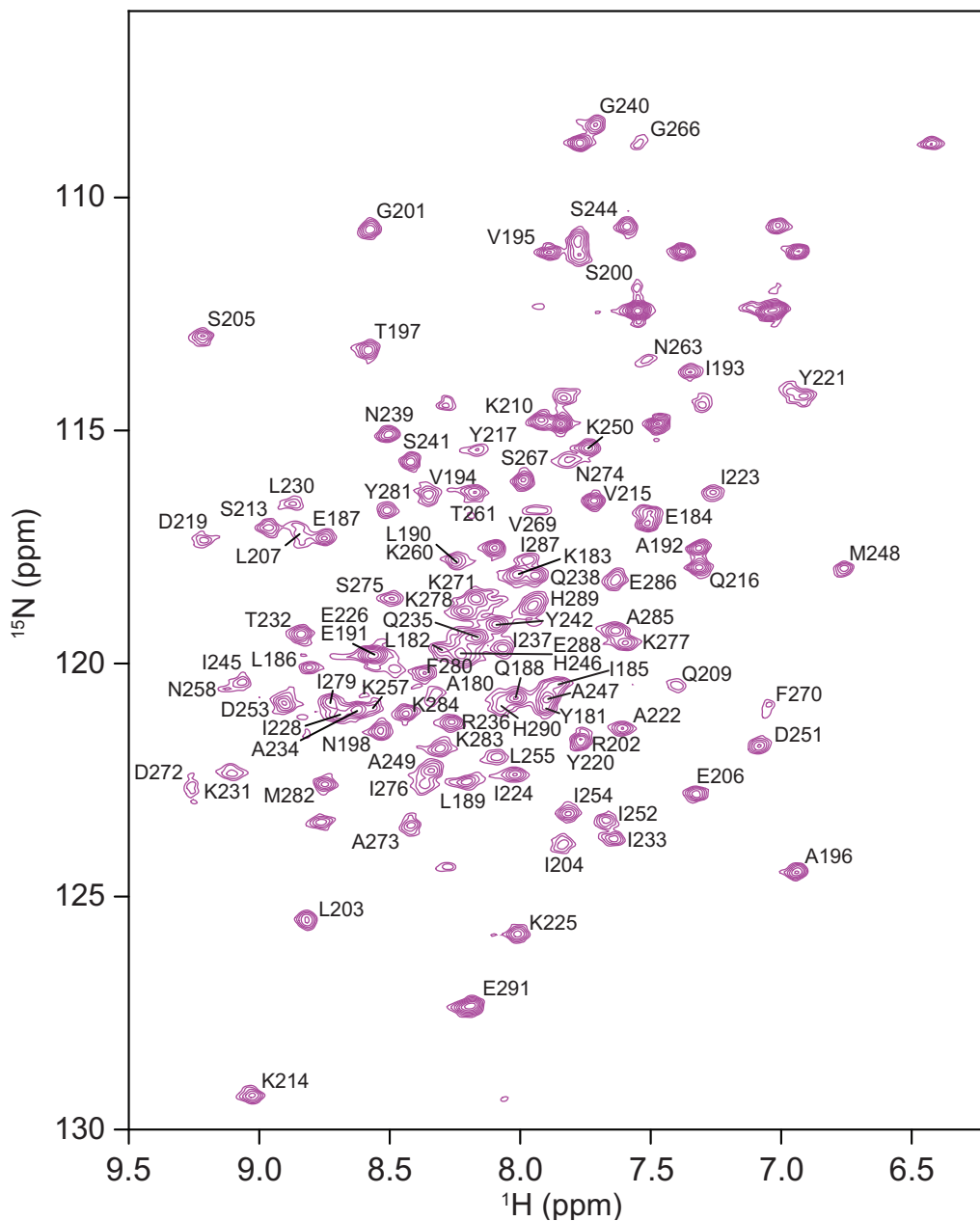
Figure S15. ^{1}H-^{15}N HSQC spectrum of U-^{15}N-PBRM1-BD2 (600 µM), in presence of **16** (750 µM), with resonances labeled with their amino acid assignments. The chemical shifts for these assignments were deposited in the Biological Magnetic Resonance Bank (BMRB ID 51450).
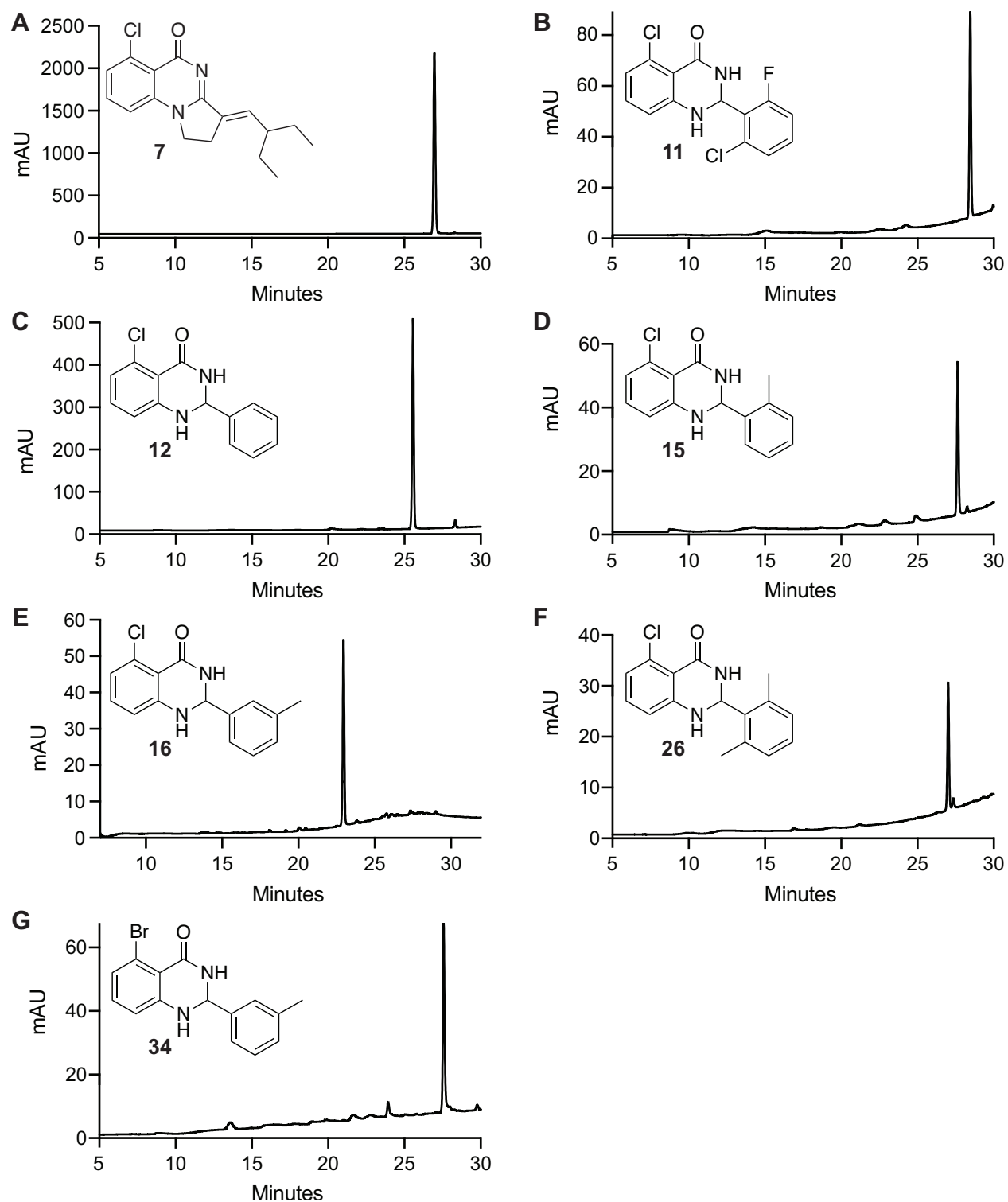
Figure S16. HPLC chromatograms of promising lead PBRM1 bromodomain inhibitors evaluated in cellular assays. The peak with the greatest magnitude on each chromotagram corresponds to the respective compound with >95% purity. (A) Compound **7**. (B) Compound **11**. (C) Compound **12**. (D) Compound **15**. (E) Compound **16**. (F) Compound **26**. (G) Compound **34**.

Table S1. Comparison of the ability of our synthesized PBRM1-BD2 inhibitors (**15**, **16**, **25**, **26**, and **34**) vs. literature reported PBRM1-BD5 inhibitors (**2** and **7**) to stabilize bromodomains belonging to different bromodomain subfamilies as observed by differential scanning fluorimetry (DSF) assays.
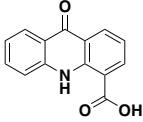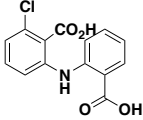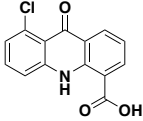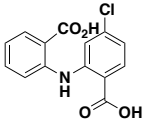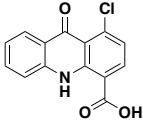
ΔT_m (°C)	< 1	1-2	2-3	3-5	>5

Compound	PBRM1-BD1	PBRM1-BD2[a]	PBRM1-BD3	PBRM1-BD4	PBRM1-BD5	PBRM1-BD6	SMARCA2B	SMARCA4	ASH1L	TRIM33B	BRD7
2	-0.1	3.3 ± 0.4	2.6	0.3	7.7	-1.4	2.2	2	-0.7	-0.9	1.2
7	-0.9	7.7 ± 0.2	2.8	3.9	11.0	-1.5	3.0	3.1	-0.7	0.3	0.4
15	-0.8	5.4 ± 0.1	2.7	0.9	2.9	-2	0.5	0.4	-0.6	0.8	0.2
16	-0.1	5.4 ± 0.2	1.8	0.8	1.8	-1.9	0.4	0.3	-0.6	0.9	0.0
25	-0.3	3.9 ± 0.3	1.9	0.2	0.9	-1.3	0.0	-0.4	-0.8	0.3	0.0
26	-0.5	5.2 ± 0.3	5.0	1.0	4.4	-1.2	0.5	0.6	-0.8	0.5	0.1
34	1.4	6.4 ± 0.2	0.6	0.2	1.5	-2.4	0.3	-0.2	-0.4	0.1	-0.4

| Compound	CREBBP	p300	BRD2-BD2	BRD3-BD1	BRD3-BD2	BRD4-BD1	BRD4-BD2	BRDT-BD1	CECR2	PCAF
2	0.1	-0.6	-0.2	0.1	0.5	0.1	-0.6	-0.1	2.0	-0.2
7	-0.7	-0.5	0.6	-0.3	0.4	-0.2	-1.1	-0.8	-0.9	0.4
15	0.5	0.2	0.6	0.3	0.4	0.1	-3.3	-0.7	-0.5	0.5
16	0.4	-0.2	0.6	0.3	0.4	0.3	-3.9	-0.1	-1.3	0.5
25	0.6	0.6	0.2	0.4	0.4	0.6	-4.2	0.1	0.8	0.1
26	0.2	0.2	0.5	0.0	0.3	0	-4.4	-0.6	1.3	0.6
34	-0.2	-0.1	0.5	0.4	0.5	0.3	-1.1	-0.4	-0.6	0.6

[a]Values shown are the average of triplicates.

Table S2. Binding of the analogs of the second-best hit (**6**) to PBRM1-BD2 as observed by DSF and AlphaScreen assays.
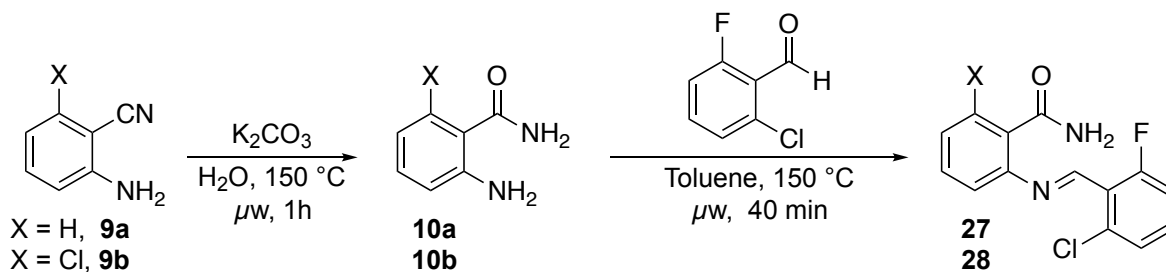
Compound	Structure	PBRM1-BD2 ΔT_m (°C)	IC$_{50}$ values (μM)
6		1.5 ± 1.0	127 ± 30[a]
36		1.4 ± 0.2	26[b]
37		3.0 ± 0.1	7[b]
38		0.3 ± 0.02	>250[b]
39		0	>250[b]

[a]Values shown are the average of triplicate. [b]Values shown are single replicate.
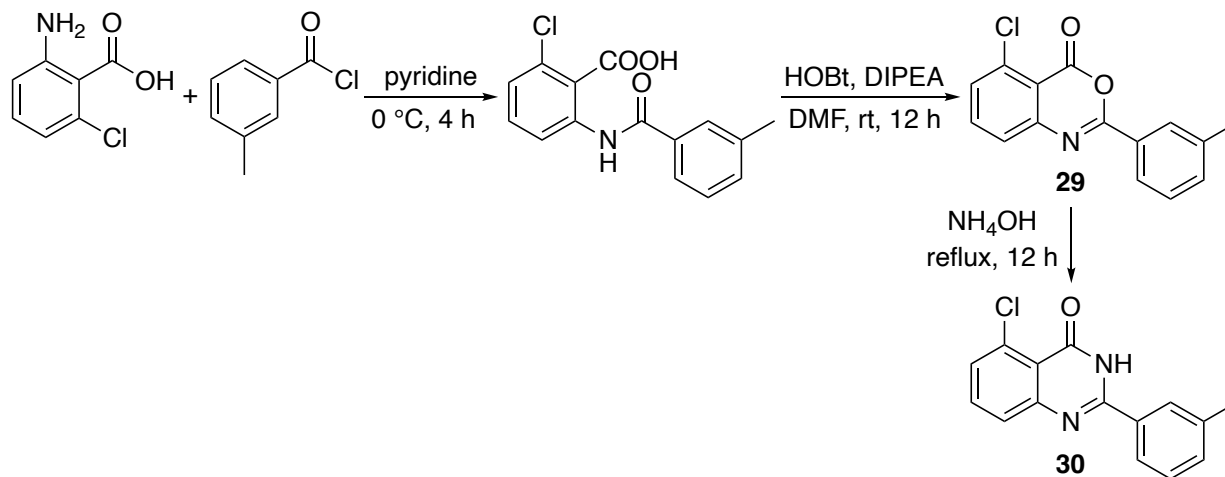
Scheme S1. Synthetic route to compounds **7** and **8**.[1]
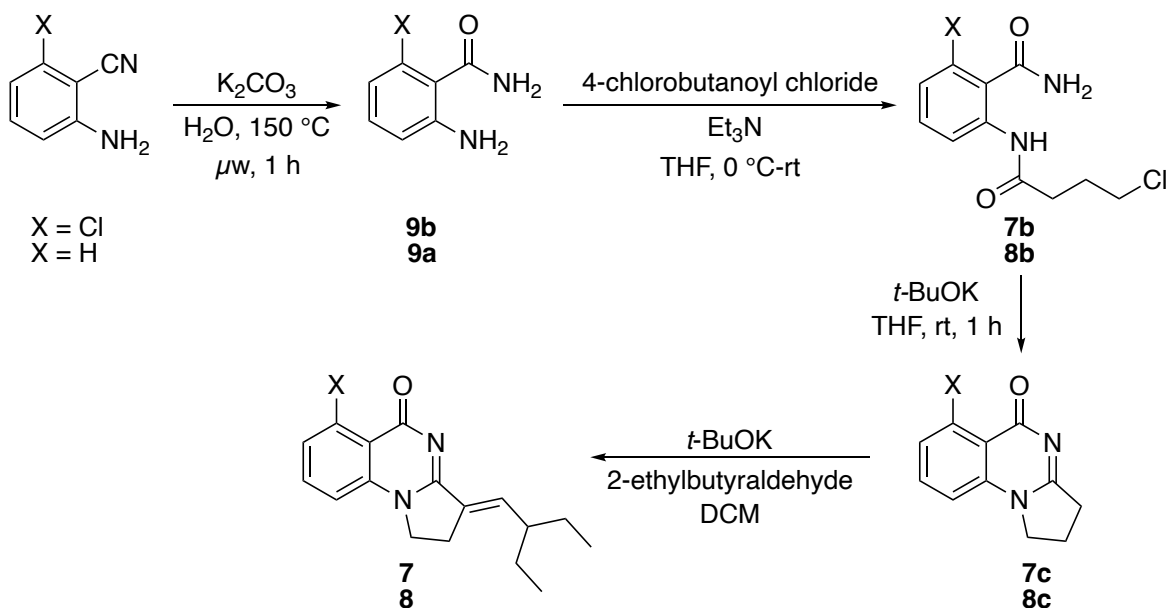
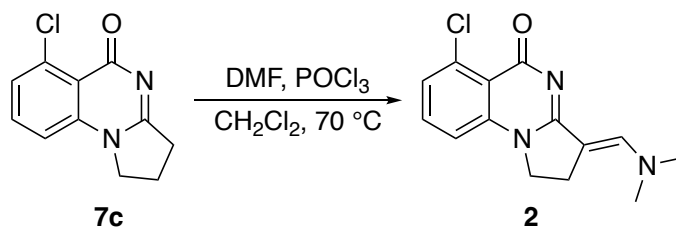**Scheme S2.** Synthetic route to compounds **27** and **28**.

Scheme S3. Synthetic route to benzoxazin-4-one[2] (**29**) and quinazolin-4-one[3] (**30**).
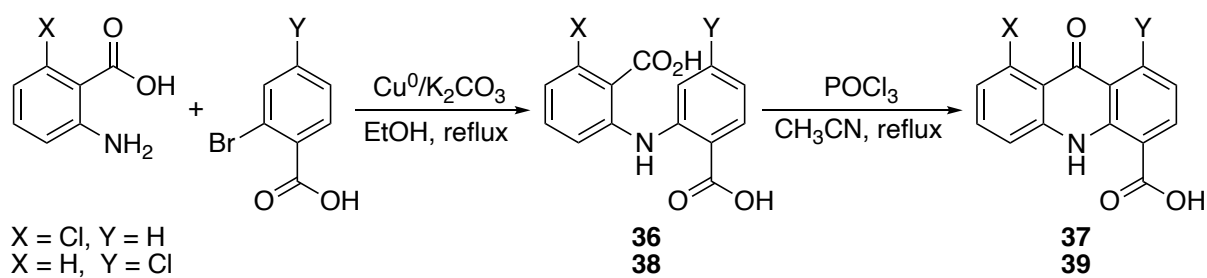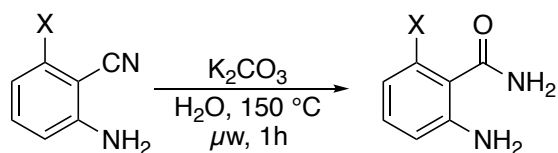
Scheme S4. Synthetic route to literature compound **2**.[1]

7c → **2**

DMF, POCl$_3$
CH$_2$Cl$_2$, 70 °C

Scheme S5. Synthetic route to analogs of **6**.[4]

X = Cl, Y = H
X = H, Y = Cl

Cu^0/K$_2$CO$_3$
EtOH, reflux

36
38

POCl$_3$
CH$_3$CN, reflux

37
39

Scheme S6. General Procedure A: Synthesis of aminobenzamides.[1]

K$_2$CO$_3$
H$_2$O, 150 °C
μw, 1h

Scheme S7. General Procedure B: Synthesis of 2,3-dihydroquinazalinones.[5]

0.2 M aq. KOH (2 mL)
DMSO (1 mL), rt
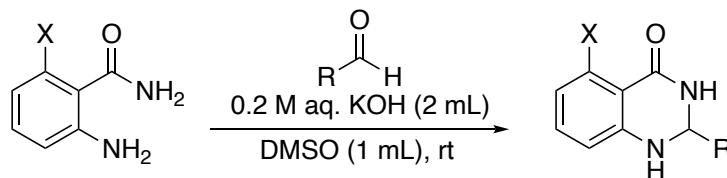
References

1. Sutherell, C. L.; Tallant, C.; Monteiro, O. P.; Yapp, C.; Fuchs, J. E.; Fedorov, O.; Siejka, P.; Müller, S.; Knapp, S.; Brenton, J. D.; Brennan, P. E.; Ley, S. V. Identification and Development of 2,3-Dihydropyrrolo[1,2-a]quinazolin-5(1H)-one Inhibitors Targeting Bromodomains within the Switch/Sucrose Nonfermenting Complex. *Journal of Medicinal Chemistry* **2016,** 59, 5095-5101.
2. Jin, S.; Liu, Z.; Milburn, C.; Tomaszewski, M.; Walpole, C.; Wei, Z.-Y.; Yang, H. Preparation of Benzamide Derivatives for Therapeutic Use as Cannabinoid Receptor Modulators. WO2005115972A1, 2005.
3. Pieterse, L.; Van Der Walt, M. M.; Terre'Blanche, G. C2-Substituted Quinazolinone Derivatives Exhibit A_1 and/or A_{2A} Adenosine Receptor Affinities in the Low Micromolar Range. *Bioorganic & Medicinal Chemistry Letters* **2020,** 30, 127274.
4. Dörner, B.; Kuntner, C.; Bankstahl, J. P.; Wanek, T.; Bankstahl, M.; Stanek, J.; Müllauer, J.; Bauer, F.; Mairinger, S.; Löscher, W.; Miller, D. W.; Chiba, P.; Müller, M.; Erker, T.; Langer, O. Radiosynthesis and in Vivo Evaluation of 1-[18F]fluoroelacridar as a Positron Emission Tomography Tracer for P-Glycoprotein and Breast Cancer Resistance Protein. *Bioorganic & Medicinal Chemistry* **2011,** 19, 2190-2198.
5. Dutta, A.; Damarla, K.; Bordoloi, A.; Kumar, A.; Sarma, D. Koh/Dmso: A Basic Suspension for Transition Metal-Free Tandem Synthesis of 2,3-Dihydroquinazolin-4(1H)-ones. *Tetrahedron Letters* **2019,** 60, 1614-1619.